The concept of the MCAO upgrade for the Daniel K. Inouye Solar Telescope

Dirk Schmidt[1], Thomas Rimmele[1], Jose Marino[1],
Luke C. Johnson[1], Steve Hegwer[1], Nicolas Gorceix[2],

[1)] National Solar Observatory, 3665 Discovery Drive, Boulder, CO 80303, USA
[2)] Big Bear Solar Observatory, 40386 North Shore Lane, Big Bear City, CA 92315, USA

ABSTRACT

The 4-meter Daniel K. Inouye Solar Telescope shall be upgraded with a mirror multi-conjugate adaptive optics system a few years after first light, replacing its initial high-order single conjugate system. We present the technical concept of this system and its subsystems. The system design sports three deformable mirrors, nine correlating Shack-Hartmann wavefront sensors, and a computer cluster for the control loop. We discuss the demands and challenges as well as our plans to implement the wavefront sensing and control systems.

1. INTRODUCTION AND MOTIVATION

High-resolution imaging, in both the spatial and temporal domain, of complete active regions on the sun at or near the diffraction limit of a 4-meter telescope is critical for the observation and analysis of the underlying physical processes. The 4-meter Daniel K. Inouye Solar Telescope (DKIST), which is currently being completed by the U. S. National Science Foundation's National Solar Observatory (NSO) at the Haleakala Observatory on the Hawaiian island of Maui, shall be upgraded with a multi-conjugate adaptive optics (MCAO) system a few years after commissioning. MCAO is an advanced adaptive optics (AO) technology.[1–3] It aims to correct for the degradation of the image of an astronomical object in a ground-based telescope caused by fluctuations of the refractive index in the atmosphere.[4,5] This atmospheric effect is known as *seeing* in the astronomical community. Correction of the seeing over a field of view of dozens of arcseconds is important to capture the fast dynamics in large active regions.

A classical, single-conjugate AO system utilizes one deformable mirror to compensate for the seeing. This mirror is placed in a pupil and applies the same correction to any point in the field of view. This is a well established, mature technology that has been used in everyday observations at most solar telescope for over a decade and is considered to be the prime enabling technology of optical solar telescopes with apertures larger than one meter.[6,7] Atmospheric disturbances, however, are anisotropic, and the correction of a single conjugate system is typically only good over a small angle that depends on the momentary vertical profile of the seeing. A multi-conjugate system uses a number of deformable mirrors, each conjugate to a different atmospheric altitude, to apply different correction to different viewing directions and to effectively correct a larger angular volume of the atmosphere. A great amount of research and development in the field of MCAO has been conducted over the past two decades at institutions around the world. An excellent overview of the current state of the art can be found in Reference 1.

The first experiments with MCAO for solar observations, using two deformable mirrors, were conducted at the Vacuum Tower Telescope on Tenerife of the then German Kiepenheuer Institute (now Leibniz Institute) for Solarphysics and at NSO's Dunn Solar Telescope in the United States in the mid 2000's.[8,9] An MCAO system with three deformable mirrors was developed and installed by the Leibniz Institute at the solar telescope Gregor on Tenerife in 2013 but removed from the telescope after one year.[10,11] Also in 2013, the National Solar Observatory teamed up with the New Jersey Institute of Technology, and with the then Kiepenheuer Institute to advance MCAO for solar observations with DKIST. The solar MCAO pathfinder system "Clear" was built and installed at the 1.6-meter Goode Solar Telescope, which—like DKIST—is a clear-aperture off-axis Gregory telescope.[12–15] Clear is an ultra-flexible MCAO system with three deformable mirrors and has been

Send correspondence via e-mail to Dirk Schmidt (dschmidt@nso.edu)

used to identify the approach for the MCAO system for DKIST. Clear has proven the power of MCAO for solar observations and impressively demonstrates high-order image correction over an area that is about 9 times as large as the area obtained by classical, single conjugate correction.[16] The concept for DKIST MCAO presented in this paper is directly based on this work.

At first light, DKIST will sport "HOAO", which is a classical, single-conjugate AO system with 1600 actuators and 1457 subapertures that supports all instruments on the coudé platform.[17–21] HOAO shall be replaced after a few years by the MCAO system presented in this paper. DKIST's HOAO is a very complex system and inherited many concepts from the "AO76" system of the 0.76-cm Dunn Solar Telescope and is essentially a scaled up and modernized version thereof. Limitations in image sensor and computing technologies impede a straightforward scaling up of Clear to the dimensions of DKIST, and a much more complex and challenging design is required to establish MCAO at a 4-meter telescope than it is at a 1.6-meter counterpart.

2. MCAO FOR DKIST

2.1 Basic parameters

The first generation MCAO for DKIST as presented in this paper is a trade-off of complexity (cost, time to build, integration, and modifications) and the seeing conditions targeted. This first generation system design includes three deformable mirrors conjugate to 0, 4, and 11 km, and nine correlating Shack-Hartmann wavefront sensors. The field of view of the MCAO correction is up to 60 arcsec in diameter. The existing deformable mirror of the HOAO conjugate to the pupil will be reused. The high-altitude deformable mirrors will replace existing folding flats in the optical train. The subapertures in the wavefront sensor measure 9.3 cm and have the same size as in the HOAO wavefront sensor. This size is matched to the actuator pitch in the pupil-conjugate deformable mirror. Only the 41 subapertures out of 43 across the pupil are used in MCAO mode to evade the effects from pupil distortion in edge subapertures that occurs in a telescope with deformable mirrors that are not conjugate to the pupil. This is 1313 subapertures per wavefront sensor and a total of 11817 in all sensors. All 43 subapertures along the pupil diameter will be used in both classical and ground-layer AO mode. An example of the expected performance is shown in Figure 1.

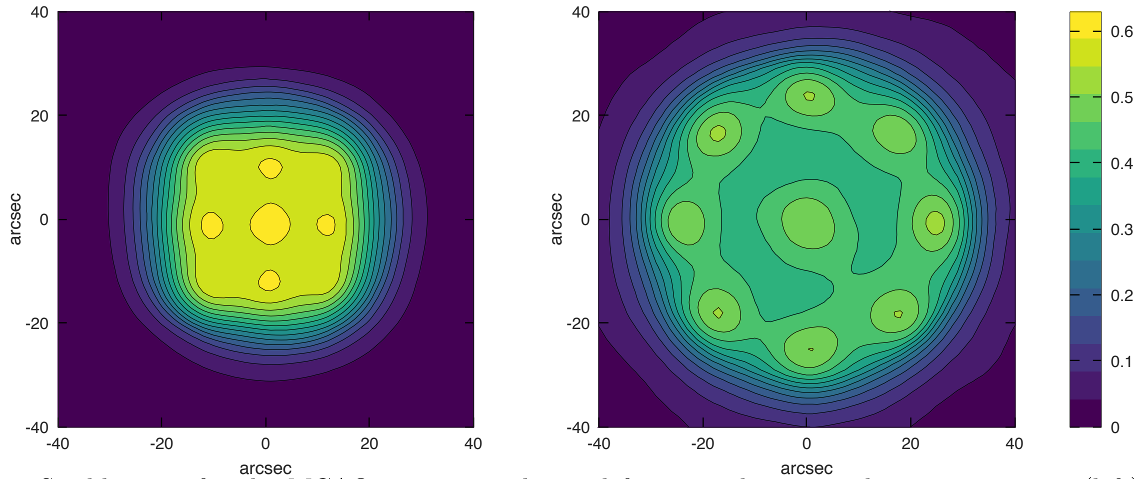

Figure 1: Strehl ratios for the MCAO correction obtained from simulations with a 35×35 arcsec (left) and a ⌀60 arcsec (right) field of view in the wavefront sensor system with the DKIST median turbulence profile and $r_0 = 15$ cm at 30° elevation. Plots show the average Strehl ratios of 100 random samples.

2.2 The wavefront sensor assembly

Until now, Shack-Hartmann wavefront sensing in solar MCAO was performed using wide-field wavefront sensor assemblies built around a single micro-lens array and a single camera.[22] The lack of readily available suitably fast and large CMOS sensors that could be used to build a wide-field wavefront sensor with a single camera for a 4-meter aperture prohibits to scale up the wavefront sensor assembly of Clear.[23] The wavefront sensor system for DKIST MCAO is divided into nine optically identical copies with a 10×10 arcsec field of view as shown in Figure 2. Each copy is pointed at a different direction (referred to as guide region) on the sun and loaded with its own fast CMOS camera. The optical designs of the first air-spaced triplet and of the microlens array are identical to the components in the DKIST HOAO wavefront sensor. The optic that relays the image from the microlens array focus onto the camera will be optimized for the pixel size of the final camera model that is yet to be determined.

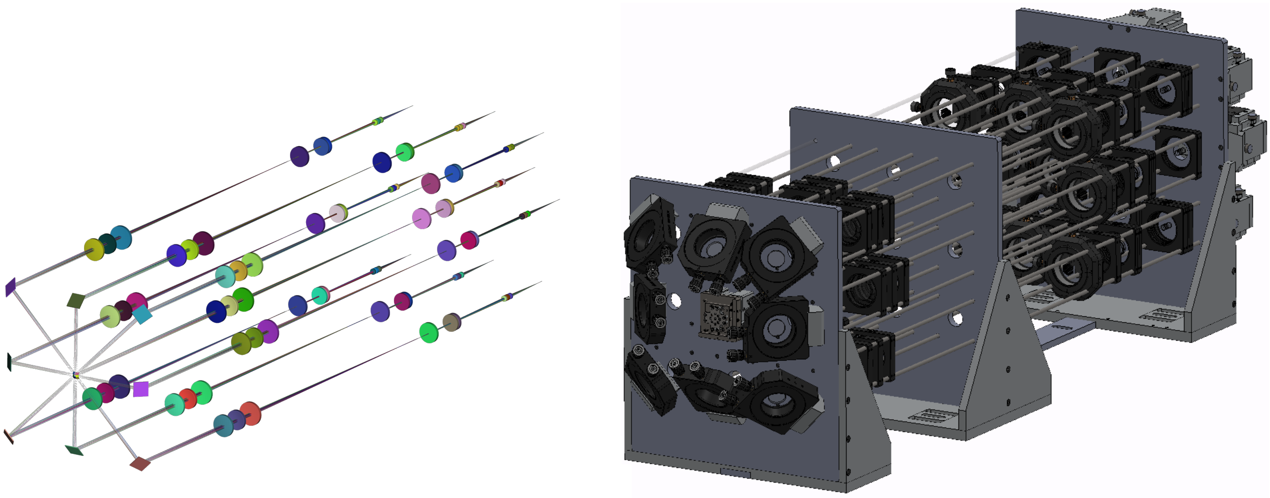

Figure 2: The working design of a prototype of the DKIST MCAO wavefront sensor assembly. The assembly includes 3×3 separate Shack-Hartmann wavefront sensors with with 10×10 arcsec field of view, each pointing in a different direction.

2.2.1 Guide-region light distribution

The light for each of the eight off-axis wavefront sensors is picked up in the focal plane with eight 45°-mirrors that serve as reflective field stops as shown in Figure 3. By modifying the spacing of the mirror elements, different regions in the field of view can be selected. Because the field stop is tilted by 45° with respect to the image plane, some portions of the field stop are slightly blurred in consecutive image planes such as the final detector plane. This effectively introduces vignetting that needs to be accounted for in the design as is explained below.

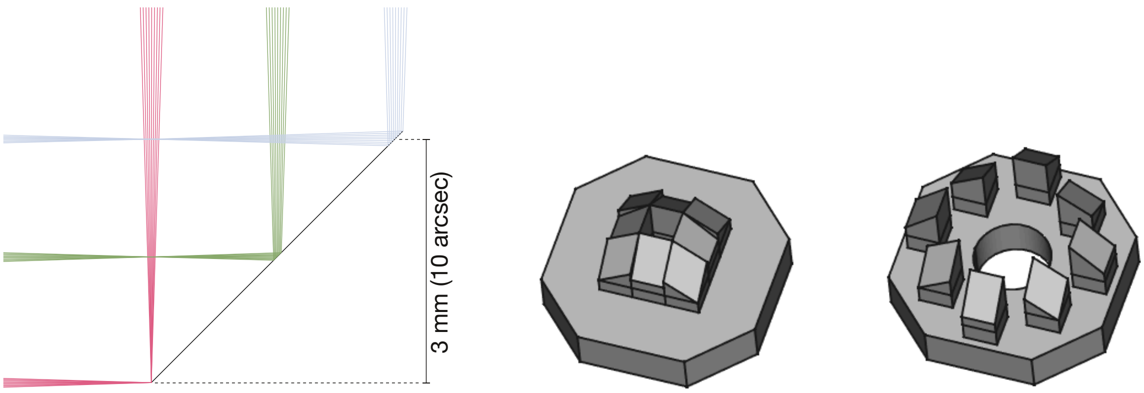

Figure 3: Principle of the guide-region pick-up mirror device. Side view of a mirror in a focal plane tilted by 45°(left), and two complete assemblies for a field of view of ≈35×35 arcsec (middle), and ⌀60 arcsec (right). Each mirror picks up about 10×10 arcsec from the focal plane.

The guide-region pick-up mirror concept has a number of upsides:

1. A change of the wavefront correction beamsplitter in DKIST does not become immediately necessary with the wide-field AO upgrade. Additional beamsplitters are avoided and photons in any field point are directed onto one wavefront sensor camera. Thus the field segmentor makes optimal use of the incoming light.

2. The optical design of the existing DKIST high-order wavefront sensor can be re-used and components re-made without re-engineering minimizing both development costs and project duration.

3. The span of the guide-regions can be changed by placing the mirrors further apart without implications on detector sizes. This opens up in particular the option to build a very wide-field wavefront sensor for a ground layer AO mode.

4. The central wavefront sensor can be used to run classical AO control similar to the DKIST first light HOAO system.

5. The photon flux on each wavefront sensor camera can be adjusted independently of the others for optimal signal-to-noise ratios, e. g. if there is a sunspot in the field of view of a sensor.

6. Each wavefront sensor can be focussed individually to adapt to the field curvature in the DKIST WFC focus.

A downside of a tilted field stop in a Shack-Hartmann wavefront sensor is the field of view reduction shown in Figure 4. This effectively requires a wavefront sensor design [24, Appendix A] for a larger field of view than nominal and a larger detector than in a Shack-Hartmann with an upright field stop. The simulated image plane in a wavefront sensor like in DKIST MCAO with a tilted field stop is shown in Figure 5 and Figure 6. The simulations indicate that a 10–15% larger detector is needed to preserve the same effective field of view as in a wavefront sensor with an upright field stop. This effect can be avoided if the guide region pick-up mirrors are sufficiently far apart such that the mirrors can be oversized and an upright field be used just in front of the mirror.

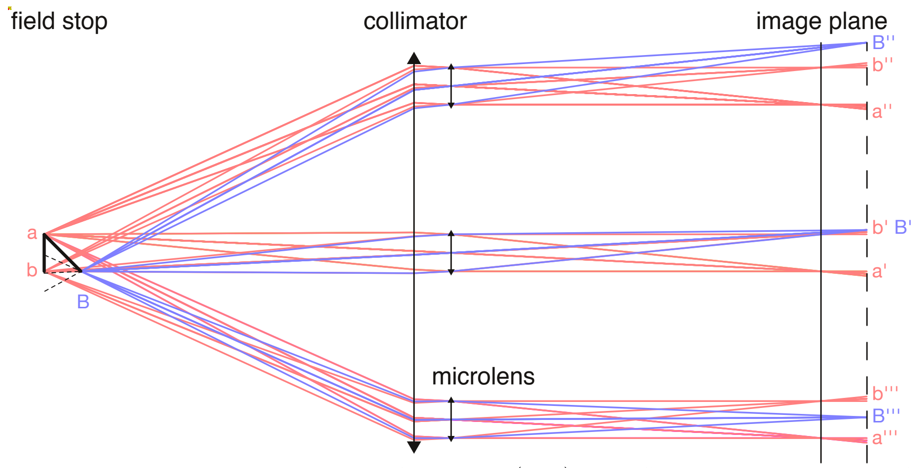

Figure 4: Field of view reduction due to a tilted field stop (a-B) in a Shack-Hartmann wavefront sensor. The ray tracing shows the locations of the images of the field stop edge in three subapertures. The images (B′, B″, B‴) out-of-focus edge (B) of the field stop are displaced with respect to the images (b′, b″, b‴) of the in-focus edge (b). In the upper half of the image plane, the image of the titled field stop is larger and in the lower half smaller than the image of the upright field stop (a-b). In addition to the displacement, the image of the out-of-focus edge is slightly blurred. While the size of image of the tilted field stop depends on the distance of the subaperture from the optical axis, the magnification in the image plane does not change. Consequently, the transmitted field of view is clipped in the lower half and expanded in the upper half.

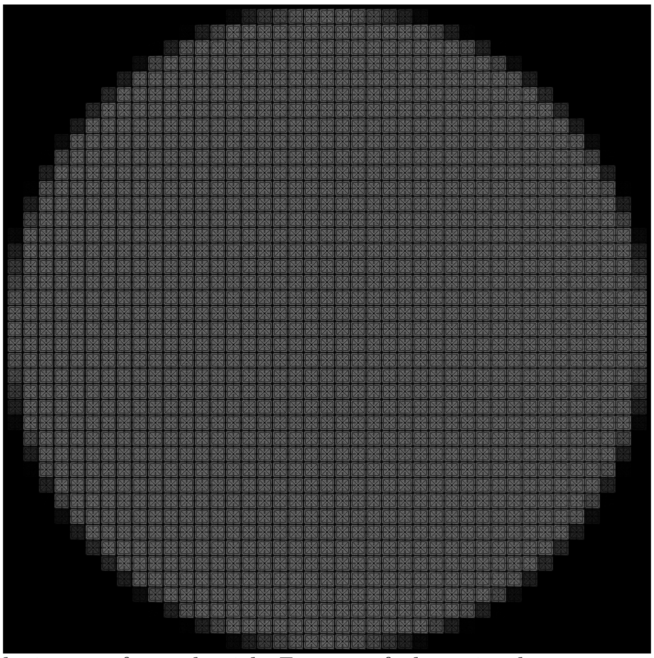

Figure 5: Geometrical simulation performed with Zemax of the microlens array image plane in the DKIST HO-WFS with a 20.5 mm pupil (41 suapertures) with a 2.8382×4.0138 mm field stop tilted by 45° (left-hand side edge is in focus, right-hand side edge is out of focus). See Figure 6 for close-ups.

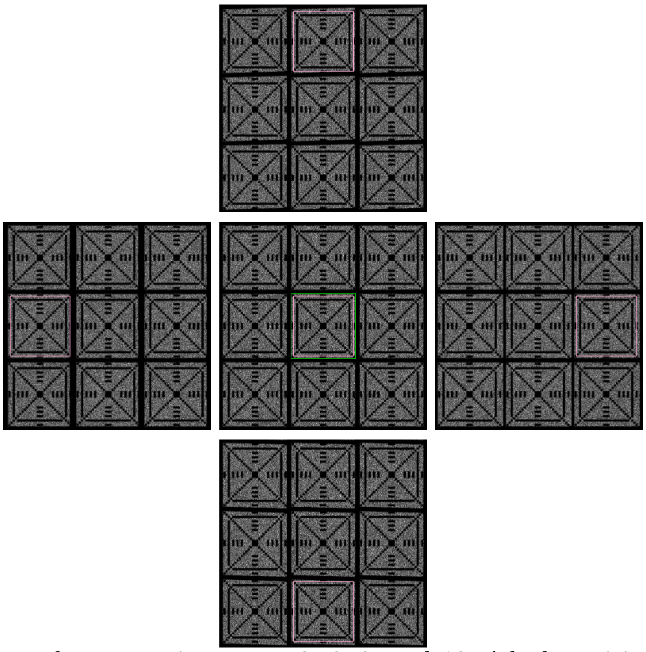

Figure 6: The 3×3 outermost subaperture images at 3, 6, 9, and 12 o'clock position as well as the central 3×3 subapertures in Figure 5. As demonstrated in Figure 4, the out-of-focus edge of the field stop on the right appears at different positions depending on the subaperture's radial position which becomes visible by horizontal gaps of different widths. The horizontal edges of the field stop appear tilted in some subapertures.

A prototype to verify this concept experimentally is to be set up at NSO's lab in Boulder. The guide-region pick-up mirror device, shown in Figure 7, was manufactured by BMV Optical Technologies* and has been shipped to Boulder.

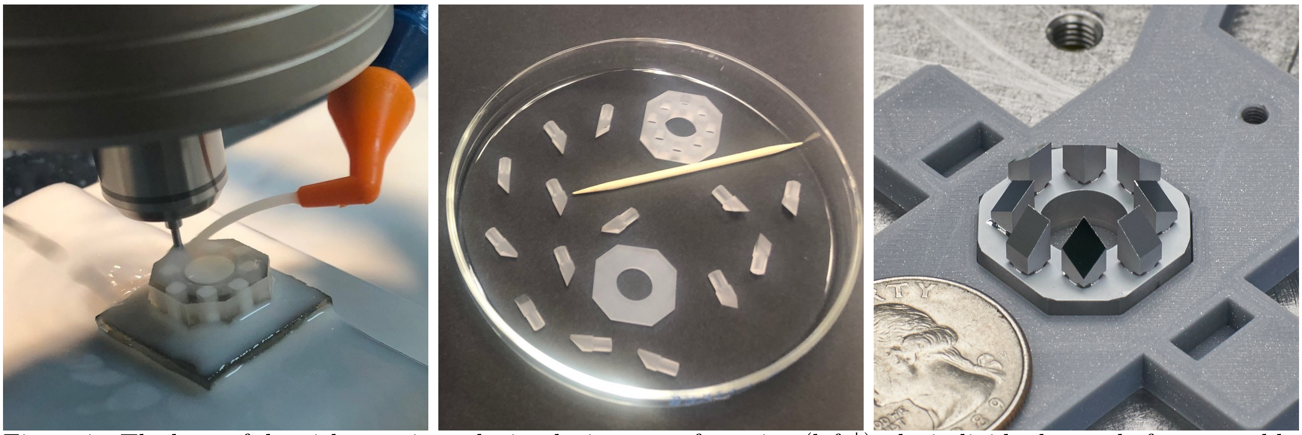

Figure 7: The base of the pick-up mirror device during manufacturing (left*), the individual parts before assembly (center*) and the coated device after delivery to NSO (right). *) courtesy of BMV Optical Technologies

2.2.2 Wavefront sensor cameras

Some key requirements specific to the cameras in the wavefront sensor are listed in Table 1. We are unaware of a currently commercially available camera that meets all goals in this table. The Mikrotron EoSens 3CXP is readily available and we have been using this camera successfully in the wavefront sensor in Clear. Its specifications are close to the the minimum requirements. We therefore plan to use this model in the beginning. We anticipate prompt advances in the camera industry, and we plan to buy customized cameras that meet all requirements. Figure 8 shows the shot noise and the quantization noise of the camera as a function of the full well capacity. With an exemplified full well capacity of 40 ke$^-$, the 8-bit quantization noise is approximately 45 e$^-$ which adds about 2% to the noise near saturation; about 0.5% is added with 9-bit quantization. The cameras will be operated at high exposure levels, and we expect read-noise and dark current to be negligible contributors to the total noise.

Table 1: Top-level requirements for a wavefront sensor camera

	requirement	Mikrotron EoSens 3CXP[25]
sensor read-out size	>1000×1000 px	1696×1710 px
frame rate	>1500 fps, goal >2000 fps	1513 fps, 1024×1000 px
interface	real-time streaming to Linux host	CoaXPress
shutter type	global	global
full well capacity	>30 ke$^-$, goal >60 ke$^-$	27 ke$^-$
read-noise	<30 e$^-$, goal <15 e$^-$	21 e$^-$
quantization	8, 9, or 10 bit ($\leq$ 16 bit ok)	8 bit

2.3 Deformable mirrors

The MCAO upgrade may not reduce the field of view delivered to various instruments which may be larger than what is corrected by the MCAO. Therefore, the face sheets of $DM_{4\ km}$ (replacing M9) and $DM_{11\ km}$ (replacing Mz) are significantly larger than the area with actuators as shown in Figure 9. The folding flats M7 and M9 pass 5 and 2.8 arcmin fields of view, respectively. Specifics of the deformable mirror are listed in Table 2. $DM_{0\ km}$ is installed in DKIST and waiting for the first light while this is being written. $DM_{4\ km}$ has been contracted with AOA Xinetics† and is being manufactured. They are also conducting a design study for $DM_{11\ km}$.

*BMV Optical Technologies, Otawa, Canada. `https://www.bmvoptical.com`

†AOA Xinetics, Devens, MA, USA. `https://www.northropgrumman.com/BusinessVentures/AOAXinetics/`

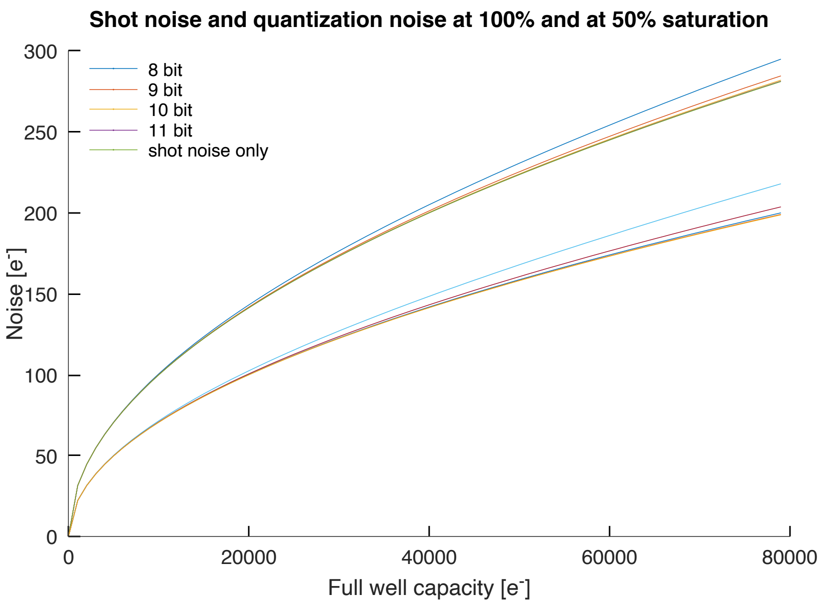

Figure 8: Shot noise ($\sigma_\mathrm{s} = \sqrt{\text{number of e}^-}$) and quantization noise[26] ($\sigma_\mathrm{q} = 1/\sqrt{12}\cdot$ number of e^- per least significant bit) are the main sources of pixel noise in the wavefront sensor camera image. Plotted is $\sqrt{\sigma_\mathrm{s}^2 + \sigma_\mathrm{q}^2}$ for 100% saturation (upper lines) and for 50% saturation (lower lines). Linear quantization from 0 e^- to full well capacity is assumed.

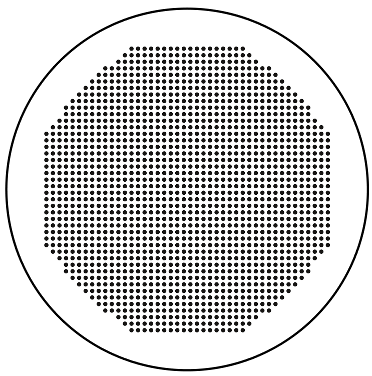

Figure 9: Actuator layout and clear aperture of $\mathrm{DM}_{4\ \mathrm{km}}$ (see also Table 2).

Table 2: Deformable mirrors

MCAO mirror designation	$\mathrm{DM}_{0\ \mathrm{km}}$	$\mathrm{DM}_{4\ \mathrm{km}}$	$\mathrm{DM}_{11\ \mathrm{km}}$
DKIST mirror designation	M10	M9	M7
conjugate distance	0 km	4.3 km	11.2 km
number of actuators	1600	1600	TBD (presum. <800)
actuator pitch	4.8 mm	7.02 mm	TBD
pitch at conjugate	9.3 cm	12 cm	TBD
clear aperture	210 mm	388 mm (2.8 arcmin)	884 × 625 mm elliptical (5 arcmin, 45 angle of incidence)
controlled aperture	210 mm	302 mm	316 × 223 mm elliptical
technology	Xinetics SNA	Xinetics SNA	TBD
status (10/2019)	installed at DKIST	in production	design study at NGC AOA/Xinetics

2.4 Real-time control system

Two different hardware architectures have been recently used for real-time controlers (RTCs) in solar AO: Entirely CPU based systems utilizing server-class computers with x86-64 processors (e. g. KAOS Evo 2), and FPGA/CPU hybrids (e. g. DKIST HOAO) in which most computations are performed by FGPAs.[7] It seems that both architectures may be used for DKIST MCAO. While the FPGA/CPU hybrid system is well suited for classical AO system with proven and established algorithms, it seems more complex to modify an FPGA-based system later. Since MCAO is still a rather young technology in solar observations, we anticipate further developments in this field and prefer an architecture with maximal flexibility. The CPU-based approach also enables us to re-use the great portions of the RTC software from Clear.

The computational demand in DKIST MCAO is driven by the matrix-vector multiplication (MVM) and not by the wavefront slope computation despite being based on image correlation. In a single-matrix wavefront reconstructor, the reconstruction matrix in DKIST MCAO is about 100 times bigger than the matrix in Clear (Table 3). This asks for a memory bandwidth that is well in excess of what is available in present shared-memory multi-socket computers or GPU accelerator boards.

We therefore choose a cluster architecture based on x86-64 computers for the DKIST MCAO RTC as shown in Figure 10. Each camera is connected to one real-time node (RTN) that computes the subaperture image shifts in the corresponding camera images and performs the corresponding chunk of the matrix-vector-multiplication as shown in Figure 11. The real-time master supervises the real-time nodes, sums up the output vectors of the RTNs and outputs the actuator commands to the drivers of the fast-steering mirror and deformable mirrors. The real-time master also sends updated reconstruction matrices to the real-time nodes. The cameras are synchronized via an external trigger signal. The cluster nodes shall be interconnected via an Infiniband EDR network for very low latency. Nodes for additional tasks, for example to update the reconstruction matrix, may be added. The approach of a x86-CPU cluster is similar to the RTC of the NFIRAOS MCAO system for the Thirty Meter Telescope.[27] Table 4 lists benchmark results that prove contemporary CPUs can be used to compute the wavefront slopes for a single DKIST MCAO wavefront sensor at a rate of 2000 fps. Table 5 lists benchmark results showing that those CPUs can be used to compute the matrix-vector multiplication. While these tables lead to the assumption that a computer with two Xeon Gold 6254 is capable of doing the wavefront sensor image processing and the matrix-vector multiplication reconstruction in parallel, we confirmed this with a modified version of KAOS Evo 2 that executes the image processing and the matrix-vector multiplication simultaneously on both CPUs without BLAS.

At this time, we have not defined what the final reconstructor for DKIST MCAO will be, in particular whether it will be a single-matrix reconstructor or a two-matrix reconstructor like in Clear. For that reason, we also list the benchmarking of a 4000×4000 matrix-vector multiplication that would be executed on the real-time master in Table 4. From this table it becomes evident that systems with sufficiently large CPU caches are needed to perform this matrix-vector multiplication quickly. A contemporary dual Intel Xeon SP Gold 6254 computer is dramatically out-performed for the MVM sizes of interest by a comparable (in terms of core-count and price) previous generation Xeon E5-2698 v4 presumably due to its larger caches despite the AVX-512, the faster clock and the higher memory bandwidth of the Cascade Lake architecture. The matrix sizes of interest for DKIST MCAO seem to fall into the weak spot of the Xeon Gold 6254. Only for significantly smaller or larger matrices (not shown but benchmarked), the Cascade Lake is able to beat the Broadwell when the matrix is either small enough to fit into its cache or large enough to benefit from the higher memory bandwidth. We currently plan to use a dual Xeon Gold 6254 computer for each of the RTN1–RTN9 computers. The specification of the RT master is being investigated and remains to be determined.

Table 3: Matrix-vector multiplication complexity in DKIST MCAO compared to other MCAO systems.

	DKIST MCAO	TMT/NFIRAOS[27]	GST/Clear
number of actuators	<4000	7673	555
number of wavefront slopes	23634	34752	1872
control matrix size (32-bit)	<380 MB	905 MB	4 MB
control loop frequency	>2000 Hz	800 Hz	1568 Hz
memory bandwidth for MVM:			
100% duty cycle	>760 GB/s	>724 GB/s	>6.3 GB/s
50% duty cycle	>1.5 TB/s	>1.4 TB/s	>12.6 GB/s
25% duty cycle	>3 TB/s	>2.8 TB/s	>25 GB/s
number of MVM cluster nodes	9	6	1
CPUs per cluster node	2× Xeon Gold 6254 (TBC)	4× Xeon Gold (TBC)	2× Xeon Gold 6154
control matrix size per node	<42.5 MB	150 MB	4 MB

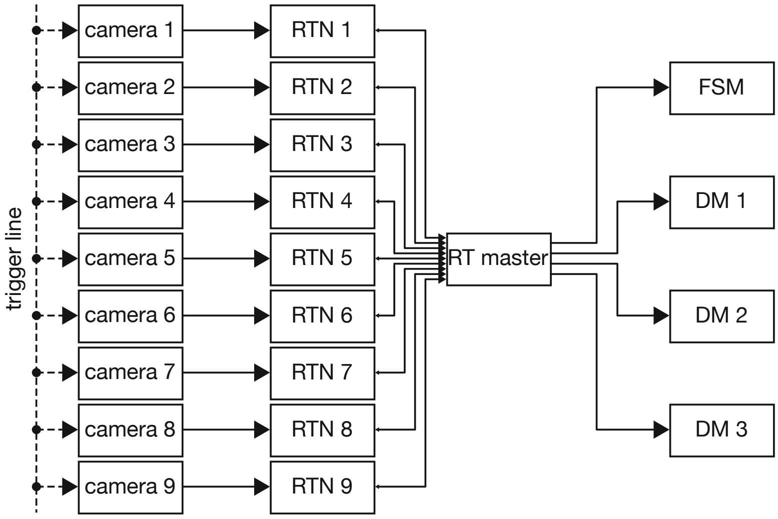

Figure 10: Scheme of RTC cluster for DKIST MCAO.

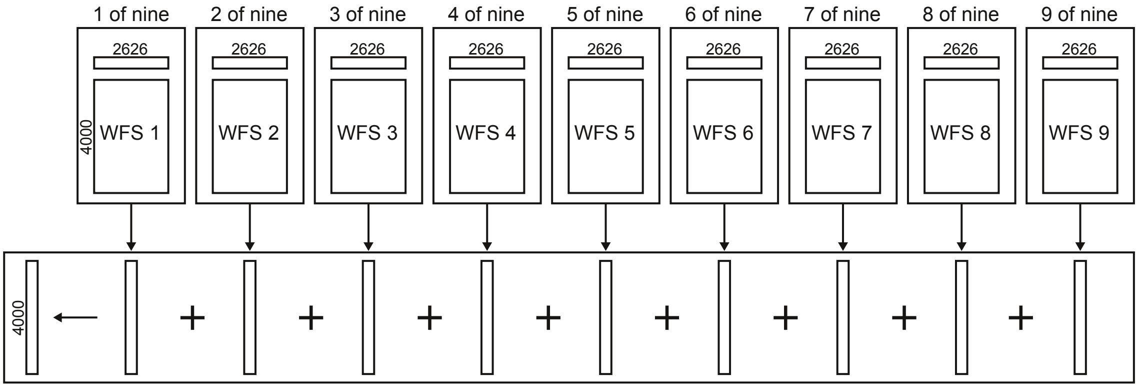

Figure 11: Parallelization of the matrix-vector multiplication in the RTC. Each Real-time Node (x of nine) computes the actuator values from the image shifts in its corresponding wavefront sensor (WFS) with a matrix-vector multiplication. The Real-time Master (unimatrix01) adds the results up.

Table 4: Benchmark results of wavefront sensor image shifts computation with the RTC in Clear and one of NSO's AO simulation computers. The minimum number of cores that is needed for various algorithms for a sustained rate of 2000 fps is listed.

computer	Tyan Thunder HX FT77DB7109	Supermicro 6018R-MT
mainboard	S7109GM2NR-2T	Super X10DRL-i
CPUs	2× Intel Xeon Gold 6154, 3.0 GHz, 18 cores, 1 MiB/core L2, 24.75 MiB L3 shared AVX, AVX2, AVX-512	2× Intel Xeon E5-2698 v4, 2.2 GHz, 20 cores, 50 MiB L3 shared AVX, AVX2
frame grabber	Active Silicon Quad CXP-6, PCIe 2.0 ×8	Euresys Coaxlink Octo, PCIe 3.0 ×8
camera	Mikrotron EoSens 3CXP	Mikrotron EoSens 3CXP
software	KAOS Evo 2 rev 1280, FFTW 3.3.6, Intel ICC 18.0.0	KAOS Evo 2 rev 1280, FFTW 3.3.8, Intel ICC 18.0.0
number of correlations	1313	1313
frame rate	2000 fps	2000 fps
correlation size	20×20 px	20×20 px
raw image size	864×860 px (8 bit)	864×860 px (8 bit)
sensor read time	<492 µs (TBC)	<492 µs (TBC)
average data rate	≈1.56 GB/s	≈1.56 GB/s
subaperture image pre-processing	dark/flat calibration, gradient removal, windowing (DFT only)	dark/flat calibration, gradient removal, windowing (DFT only)
peak interpolation	3×3 px parabolic	3×3 px parabolic
floating point precision	32 bit	32 bit
frame start to last pixel in KAOS	≈475 µs	(not measured)
DFT (not normalized)	8 cores	13 cores
DFT (normalized)	8 cores	13 cores
SDF $\pm 3 \times 3$ px	10 cores	not possible with up to 37 cores
SDF $\pm 5 \times 5$ px	17 cores	not possible with up to 37 cores
SDF $\pm 7 \times 7$ px	20 cores	not possible with up to 37 cores

Table 5: Benchmarking of matrix-vector multiplication with the BLAS function cblas_sgemv in Intel MKL on recent Intel Xeon CPUs. Timings are the average of 10000 executions after warming up the caches. GFLOP were calculated assuming $(2 \cdot n_{\text{rows}} \cdot n_{\text{cols}} - n_{\text{rows}})$ operations per MVM. (A 2014 Nvidia Tesla K80 GPU accelerator board takes around 270 µs and 400 µs, respectively for the same MVMs via cuBLAS, yielding about 80 GFLOPs/s in both cases. These times include the up- and download of the input and output vectors between the CPU and the GPU. This data transfer adds about 20-25 µs the the execution time of cublasSgemv.)

	E5-2698 v4	Gold 6254	Phi 7210	E5-4650
launch date	Q1/2016	Q2/2019	Q2/2016	Q2/2012
microarchitecture	Broadwell	Cascade Lake	Knights Landing	Sandy Bridge
status	launched	launched	discontinued	discontinued
cores	20	18	64	8
L3 cache (80%)	50 (40) MiB	24.75 (19.8) MiB	n/a	20 (16) MiB
L2 + L3 cache (80%)	n/a	42.75 (34.2) MiB	32 (25.6) MiB L2	n/a
base clock	2.2 GHz	3.1 GHz	1.3 GHz	2.7 GHz
memory bandwidth	76.8 GB/s	127.8 GB/s	102 GB/s	51.2 GB/s
instruction set	AVX2	AVX-512	AVX-512	AVX
MVM:				
4000×2626, 1 CPU (40.07 MiB)	95 µs (220 GFLOP/s)	200 µs (105 GFLOP/s)	167 µs (125 GFLOP/s)	1080 µs (20 GFLOP/s)
4000×2626, 2 CPUs (40.07 MiB)	80 µs (262 GFLOP/s)	130 µs (162 GFLOP/s)		340 µs (61 GFLOP/s)
4000×2626, 4 CPUs (40.07 MiB)				160 µs (130 GFLOP/s)
4000×4000, 1 CPU (64 MiB)	500 µs (63 GFLOP/s)	463 µs (70 GFLOP/s)	250 µs (128 GFLOP/s)	2140 µs (15 GFLOP/s)
4000×4000, 2 CPUs (64 MiB)	80 µs (400 GFLOP/s)	160 µs (200 GFLOP/s)		7600 µs (4.2 GFLOP/s)
4000×4000, 4 CPUs (64 MiB)				140 µs (227 GFLOP/s)

3. SUMMARY, STATUS & OUTLOOK

The Daniel K. Inouye Solar Telescope shall be upgraded with an MCAO system a few years after operations that serves all instruments on the coudé platform. Three deformable mirrors, at 0, 4, and 11 km, will be correcting for up to 60 arcsec in diameter. The high-altitude deformable mirrors will replace existing mirrors without any change to the optical path of the telescope. The high-order wavefront sensor system will include 9 separate cameras, each targeting at a different guide region. A computer cluster of ten x86 servers will be used to run the control loop at 2000 Hz.

The deformable mirror that will be conjugate to 4 km is being manufactured, and a design study for the 11 km mirror is being performed. We have benchmarked various computers for the real-time controller and identified the potential CPU model for the camera computers in the cluster. The guide-region pickup mirror device was manufactured. Next, we will set up a wavefront sensor prototype, and procure the computer and camera hardware. We will adapt the KAOS Evo 2 software to a cluster environment. We are looking to procure customized camera and to conclude about the design of the deformable mirror at 11 km.

ACKNOWLEDGMENTS

The National Solar Observatory (NSO) is operated and managed by the Association of Universities for Research in Astronomy (AURA), Inc. on behalf of the National Science Foundation (NSF) and the national solar and space physics research communities under a Cooperative Agreement. The mechanical design of the wavefront sensor prototype has been engineered by L. Rimmele and S. Gregory, both NSO.
We thank S. Thibault of the Université Laval in Québec, Canada, for recommending BMV Optical Technologies. DS thanks T. Berkefeld of the Leibniz Institute for Solarphysics in Freiburg, Germany, for always good discussions.

REFERENCES

[1] Rigaut, F. and Neichel, B., "Multiconjugate Adaptive Optics for Astronomy," *ARA&A* **56**, 277–314 (Sept. 2018).

[2] Dicke, R. H., "Phase-contrast detection of telescope seeing errors and their correction," *ApJ* **198**, 605–615 (June 1975).

[3] Beckers, J. M., "Increasing the Size of the Isoplanatic Patch with Multiconjugate Adaptive Optics," in [*Very Large Telescopes and their Instrumentation*], *European Southern Observatory Conference and Workshop Proceedings* **30**, 693 (1988).

[4] Davies, R. and Kasper, M., "Adaptive Optics for Astronomy," *ARA&A* **50**, 305–351 (Sep 2012).

[5] Hickson, P., "Atmospheric and adaptive optics," *A&A Rev.* **22**, 76 (Nov 2014).

[6] Rimmele, T. R. and Marino, J., "Solar Adaptive Optics," *Living Reviews in Solar Physics* **8**, 2 (June 2011).

[7] Rimmele, T., Marino, J., Schmidt, D., and Wöger, F., "Solar adaptive optics," in [*The WSPC Handbook of Astronomical Instrumentation*], Burrows, D. N., ed., WORLD SCIENTIFIC (2020).

[8] Berkefeld, T., Soltau, D., and von der Luehe, O., "Results of the multi-conjugate adaptive optics system at the German solar telescope, Tenerife," in [*Astronomical Adaptive Optics Systems and Applications II*], *Proc. SPIE* **5903**, 219–226 (Aug. 2005).

[9] Rimmele, T., Richards, K., Roche, J., Hegwer, S., and Tritschler, A., "Progress with solar multi-conjugate adaptive optics at NSO," in [*Advances in Adaptive Optics II*], *Proc. SPIE* **6272**, 627206 (June 2006).

[10] Berkefeld, T., Soltau, D., Schmidt, D., and von der Lühe, O., "Adaptive optics development at the German solar telescopes," *Applied Optics* **49**, G155 (Sept. 2010).

[11] Schmidt, D., Berkefeld, T., Heidecke, F., Fischer, A., von der Lühe, O., and Soltau, D., "GREGOR MCAO looking at the Sun," in [*Adaptive Optics Systems IV*], *Proc. SPIE* **9148**, 91481T (July 2014).

[12] Schmidt, D., Gorceix, N., Zhang, X., Marino, J., Coulter, R., Shumko, S., Goode, P., Rimmele, T., and Berkefeld, T., "The multi-conjugate adaptive optics system of the New Solar Telescope at Big Bear Solar Observatory," in [*Adaptive Optics Systems IV*], *Proc. SPIE* **9148**, 91482U (July 2014).

[13] Zhang, X., Gorceix, N., Schmidt, D., Goode, P. R., Cao, W., Rimmele, T. R., and Coulter, R., "Optical design of the Big Bear Solar Observatory's multi-conjugate adaptive optics system," in [*Adaptive Optics Systems IV*], *Proc. SPIE* **9148**, 914850 (July 2014).

[14] Schmidt, D., Gorceix, N., Zhang, X., Marino, J., Goode, P., Rimmele, T., and Goode, P., "Multi-conjugate Adaptive Optics at Big Bear Solar Observatory," in [*Adaptive Optics for Extremely Large Telescopes IV (AO4ELT4)*], E33 (Oct 2015).

[15] Schmidt, D., Gorceix, N., Marino, J., Berkefeld, T., Rimmele, T., Zhang, X., Wöger, F., and Goode, P., "Progress in multi-conjugate adaptive optics at Big Bear Solar Observatory," in [*Adaptive Optics Systems V*], **9909**, 990929 (July 2016).

[16] Schmidt, D., Gorceix, N., Goode, P. R., Marino, J., Rimmele, T., Berkefeld, T., Wöger, F., Zhang, X., Rigaut, F., and von der Lühe, O., "Clear widens the field for observations of the Sun with multi-conjugate adaptive optics," *A&A* **597**, L8 (Jan. 2017).

[17] Rimmele, T., Richards, K., Roche, J. M., Hegwer, S. L., Hubbard, R. P., Hansen, E. R., Goodrich, B., and Upton, R. S., "The wavefront correction system for the Advanced Technology Solar Telescope," in [*Advances in Adaptive Optics II*], *Proc. SPIE* **6272** (July 2006).

[18] Richards, K., Rimmele, T., Hegwer, S. L., Upton, R. S., Woeger, F., Marino, J., Gregory, S., and Goodrich, B., "The adaptive optics and wavefront correction systems for the Advanced Technology Solar Telescope," in [*Adaptive Optics Systems II*], *Proc. SPIE* **7736**, 773608 (July 2010).

[19] Johnson, L. C., Cummings, K., Drobilek, M., Gregory, S., Hegwer, S., Johansson, E., Marino, J., Richards, K., Rimmele, T., Sekulic, P., and Wöger, F., "Solar adaptive optics with the DKIST: status report," in [*Adaptive Optics Systems IV*], *Proc. SPIE* **9148**, 91481S (Aug. 2014).

[20] Johnson, L. C., Cummings, K., Drobilek, M., Johansson, E., Marino, J., Richards, K., Rimmele, T., Sekulic, P., and Wöger, F., "Status of the DKIST system for solar adaptive optics," in [*Adaptive Optics Systems V*], *Proc. SPIE* **9909**, 99090Y (July 2016).

[21] Johnson, L. C., Cummings, K., Drobilek, M., Johansson, E., Marino, J., Rampy, R., Richards, K., Rimmele, T., Sekulic, P., and Wöger, F., "Laboratory integration of the DKIST wavefront correction system," in [*Adaptive Optics Systems VI*], *Society of Photo-Optical Instrumentation Engineers (SPIE) Conference Series* **10703**, 107030F (July 2018).

[22] Schmidt, D., Rimmele, T., Marino, J., and Wöger, F., "A review of solar adaptive optics," in [*Adaptive Optics Systems V*], *Proc. SPIE* **9909**, 99090X (July 2016).

[23] Schmidt, D., Marino, J., Gorceix, N., Rimmele, T., Johnson, L., Berkefeld, T., and Goode, P., "From Clear to DKIST: advancing solar MCAO from 1.6 to 4 meters," in [*Adaptive Optics Systems VI*], *Society of Photo-Optical Instrumentation Engineers (SPIE) Conference Series* **10703**, 1070326 (July 2018).

[24] Schmidt, D., Berkefeld, T., Heidecke, F., von der Lühe, O., and Soltau, D., "Testbed for the multi-conjugate adaptive optics system of the solar telescope GREGOR," in [*Astronomical and Space Optical Systems*], *Proc. SPIE* **7439** (Aug. 2009).

[25] ON Semiconductor, *LUPA3000: 3 MegaPixel High Speed CMOS Sensor* (06 2012). Rev. 9.

[26] Smith, S. W., [*The Scientist and Engineer's Guide to Digital Signal Processing*], California Technical Publishing, San Diego, CA, USA (1997).

[27] Dunn, J., Kerley, D., Smith, M., Chapin, E., Herriot, G., Veran, J.-P., Boyer, C., Wang, L., Gilles, L., and Trancho, G., "The Real-Time controller (RTC) for the Narrow Field Infrared Adaptive Optics System (NFIRAOS) for TMT final design," in [*Adaptive Optics Systems VI*], *Society of Photo-Optical Instrumentation Engineers (SPIE) Conference Series* **10703**, 1070317 (July 2018).